Petroleum Science 19 (2022) 2253–2267

Contents lists available at ScienceDirect

Petroleum Science

journal homepage: www.keaipublishing.com/en/journals/petroleum-science

Original Paper

Numerical simulation on the multiple planar fracture propagation with perforation plugging in horizontal wells

Ming-Hui Li [a, b, c], Fu-Jian Zhou [a, b, *], Bo Wang [d, **], Xiao-Dong Hu [a, b, ***], Dao-Bing Wang [e], Xiao-Ying Zhuang [c], Shao-Bo Han [c], Guo-Peng Huang [a, b]

[a] State Key Laboratory of Petroleum Resources and Prospecting, China University of Petroleum-Beijing, Beijing, 102249, China
[b] Unconventional Oil and Gas Research Institute, China University of Petroleum-Beijing, Beijing, 102249, China
[c] Institute of Photonics, Leibniz Universitat Hannover, Hannover, 30167, Germany
[d] Petroleum College, China University of Petroleum-Beijing at Karamay, Xinjiang, 834000, China
[e] Beijing Institute of Petrochemical Technology, Beijing, 102240, China

ARTICLE INFO

Article history:
Received 26 August 2021
Received in revised form
5 May 2022
Accepted 8 May 2022
Available online 13 May 2022

Edited by Yan-Hua Sun

Keywords:
Hydraulic fracturing
Multi-cluster fracture propagation
Perforation plugging
Finite element method
Fluid distribution

ABSTRACT

Intra-stage multi-cluster temporary plugging and diverting fracturing (ITPF) is one of the fastest-growing techniques to obtain uniform reservoir stimulation in shale gas reservoirs. However, propagation geometries of multiple fractures during ITPF are not clear due that the existing numerical models cannot capture the effects of perforation plugging. In this paper, a new three-dimensional FEM based on CZM was developed to investigate multiple planar fracture propagation considering perforation plugging during ITPF. Meanwhile, the fluid pipe element and its subroutine were first developed to realize the flux partitioning before or after perforation plugging. The results showed that the perforation plugging changed the original distribution of the number of perforations in each fracture, thus changing the flux partitioning after perforation plugging, which could eliminate the effect of stress interference between multiple fractures and promote a uniform fluid distribution. The standard deviation of fluid distribution in the perforation plugging case was only 8.48% of that in the non-diversion case. Furthermore, critical plugging parameters have been investigated quantitatively. Specifically, injecting more diverters will create a higher fluid pressure rise in the wellbore, which will increase the risk of wellbore integrity. Comprehensively considering pressure rise and fluid distribution, the number of diverters should be 50% of the total number of perforations (N_{pt}), whose standard deviation of fluid distribution of multiple fractures was lower than those in the cases of injecting 10%N_{pt}, 30%N_{pt} and 70%N_{pt}. The diverters should be injected at an appropriate timing, i.e. 40% or 50% of the total fracturing time (t_{ft}), whose standard deviation of the fluid distribution was only about 20% of standard deviations in the cases of injecting at 20%t_{ft} or 70%t_{ft}. A single injection with all diverters can maintain high bottom-hole pressure for a longer period and promote a more uniform fluid distribution. The standard deviation of the fluid distribution in the case of a single injection was 43.62%–55.41% of the other cases with multiple injection times. This study provides a meaningful perspective and some optimal plugging parameters on the field design during IPTF.

1. Introduction

According to EIA, hydraulically fractured wells produced three-quarters of the total gas production, yet their ultimate recovery rate (EUR) was only 25% respectively (EIA, 2018). To enhance the EUR, more and tighter hydro-fractures are created to obtain a larger stimulated reservoir volume during hydraulic fracturing in horizontal wells (Mayerhofer et al., 2008; Weijers et al., 2019). With

* Corresponding author. State Key Laboratory of Petroleum Resources and Prospecting, China University of Petroleum-Beijing, Beijing, 102249, China.
** Corresponding author.
*** Corresponding author. State Key Laboratory of Petroleum Resources and Prospecting, China University of Petroleum-Beijing, Beijing, 102249, China.
E-mail addresses: zhoufj@cup.edu.cn (F.-J. Zhou), wangbo@cupk.edu.cn (B. Wang), huxiaodong@cup.edu.cn (X.-D. Hu).

https://doi.org/10.1016/j.petsci.2022.05.004

limited horizontal well spacing, the ideal result is that multiple fractures created simultaneously all can obtain uniform fracture length. However, such results with uniform multi-fracture propagation were often not available according to the field diagnosis data (Wheaton et al., 2014, 2016; Ugueto et al., 2016; Raterman et al., 2018). Miller et al. (2011) analyzed the production logs data from numerous fracturing wells and indicated that 33% of the hydro-fractures contributed about 66% of total gas production, while 33% of the fractures contributed little to gas production (Miller et al., 2011). What's worse was that these field data also showed a serious heel-bias of fracture propagation existed when multiple fractures were created simultaneously, which increased the possibility of frac hit and had a significant negative effect on reservoir recovery (Cipolla et al., 2011; Vidma et al., 2018).

This uneven propagation phenomenon of multi-fracture has attracted a lot of attention from many scholars. Abundant numerical simulations based on displacement-discontinuity method (DDM) (Wu and Olson., 2015, 2016; Wu et al., 2017; Zhao et al., 2016; Kumar and Ghassemi, 2018), finite element method (FEM) (Shin and Sharma, 2014; Li et al., 2022a; Zeng et al., 2018), in-house method (Lecampion et al., 2015; Chen et al., 2020a, 2020b) were implemented and their results indicated that the reason caused non-uniform propagation not only came from the strong mechanical interaction (stress-shadow effect) between multiple fractures but also the nonuniform fluid distribution. Limited-entry perforation fracturing technology (LEPF) with limited perforations, was attempted to limit the flowrate in each fracture to achieve uniform multi-fracture propagation (Lagrone and Rasmussen, 1963; Cramer, 1987; Crump and Conway, 1988). Wu and Olson (2016) adopted their fully coupled fracture-propagation model to investigate how to reduce the impact of stress shadow and their results showed that smaller perforation diameter or fewer perforations in exterior clusters can promote uniform fracture growth. Similarly, Li et al. (2017) obtained similar conclusions by a three-dimensional finite element model. Somanchi et al. (2018) extended to extreme limited-entry perforation and applied fewer perforations (two or three perforations per cluster) to limit the flowrate of each fracture. However, some recent studies indicated that achieving uniform fracture propagation of multiple fractures with LEPF was still challenging because of strong perforation erosion caused by fracturing fluid with proppant, which resulted in the weaker ability to limit flowrates within multi-cluster fractures (Roberts et al., 2018, 2020; Long et al., 2018; Cramer et al., 2020).

Intra-stage temporary plugging and diverting fracturing (ITPF) is considered another potential approach to achieving uniform propagation of multi-fracture in one stage (Senters et al., 2018; Huang et al., 2018; Wang et al., 2020a; Zhou et al., 2019; Chen et al., 2020b; Zou et al., 2020). Using fracturing fluid with diverters to plug fractures or perforations of over-treated fractures that obtain large flowrates, the subsequent fluid can be diverted to flow into less-treated fractures (Wang et al., 2020b). Case studies in carbonate and sandstone reservoirs showed the diverters can successfully plug perforations and their effectiveness has been proven by post-job diagnostics and well performances (Rahim et al., 2017). More comprehensive downhole monitoring data in Haynesville Shale showed the diverters can divert the fluid to intended perforations and ITPF can promote uniform propagation of multiple fractures (Panjaitan et al., 2018). Some other field cases also proved its effectiveness to assist uniform fracture propagation (Fragachán et al., 2016; Ramurthy et al., 2016; Senters et al., 2018; Huang et al., 2018; Weddle et al., 2018). Generally, the successful application of ITPF often depends on two critical processes. Firstly, whether diverters can plug the intended perforations or fractures; Secondly, whether multi-cluster fractures can propagate more evenly after diversion. Many scholars have studied the first process by theoretical analysis and laboratory experiments. Brown et al. (1963) firstly presented a theoretical study for predicting the plugging behavior of ball sealers (one kind of diverter), and their results showed diversion occurred only when the drag force overcame the inertial force of the ball. Erbstoesser (1980) found that buoyant ball sealers can achieve highly effective diversion during well-treating operations through a lot of laboratory tests and field tests. Li et al. (2005) established a theoretical model to describe the plugging behavior of ball sealers, and they found that the plugging efficiency decreased once the perforation density increased. To determine the number of balls seating on the perforations, Nozaki and Hill (2013) proposed an empirical correlation to predict the plugged-perforation ratio through a mass of experimental data. In addition to ball sealers, combinations of different shaped and sized diverters (such as fibers and particles) were also used to plug hydro-fracture or 3D printing fractures with different openings and tortuosity (Zhang et al., 2019; Zhou et al., 2019; Yang et al., 2019; Wang et al., 2020a; Yuan et al., 2020; Li et al., 2022b; Li et al., 2022c). These studies indicated injecting a certain number of diverters can effectively plug the perforations or fractures. Once the plugging behavior occurred, another critical process is whether multiple fractures can uniformly propagate. However, due to the limitations of laboratory spaces and sample dimensions, few laboratory experiments were used to study this process. Numerical simulation is considered a very important research method. Li et al. (2020) simulated the temporarily plugging staged fracturing (TPSF) in the fractured reservoir through a finite element cohesive zone model, and their results indicated the suppressed cracks can continue to propagate by temporarily plugging. Chen et al. (2020b) numerically investigated the optimization of the number of ball sealers and the diverting timing in a heterogeneous stress reservoir by a self-developed 2D planar model, and their results indicated that more ball sealers and the earlier diverting time were required for creating a new fracture in high-stress zones. Previous studies showed that the existing numerical simulation models mainly had the following limitations: Firstly, most numerical models ignore the perforation plugging process and do not consider the flux partitioning model after perforation plugging. Secondly, few theoretical and numerical studies are conducted to investigate the effect of plugging parameters on the uniformity of multi-fracture propagation in one stage.

In this study, a 3D finite element model (FEM) based cohesive element method (CZM) was established to investigate the effect of perforation plugging on fracture propagation during ITPF. The pore-pressure cohesive element will be adopted to simulate the fracture initiation and propagation. Besides, the fluid pipe element and its subroutine based on FEM were first developed to realize the flux re-proportioning and plugging behavior after perforation plugging. Our numerical solution has been validated against an analytical solution. Then adequate simulations were conducted to investigate the plugging parameters (the number of diverters, the diverting timing, and injection frequency with the same total number of diverters) on the uniformity of fracture propagation. These results can provide helpful guidance on the design of plugging parameters during ITPF.

2. Mathematical model

2.1. Assumptions

Simultaneous propagation of multi-cluster hydraulic fracture is an extremely complex problem during ITPF (Wang et al., 2020a). Some reasonable assumptions and simplifications can be made in this paper. Firstly, hydraulic fractures are planar fractures without curving which is reasonable in our model because fractures will

propagate approximately like this pattern in a larger *in-situ* horizontal differential stress (such as over 4 MPa) (Li et al., 2017). Secondly, the diverters are evenly distributed in the fracturing fluid, and each diverter can only plug one perforation. Thirdly, proppant distribution and perforation erosion are not considered in this model as they are not the focus of this paper. Finally, the fluid friction in the horizontal wellbore has been neglected in our study because the fluid friction in one stage (usually less than 100 m) is small compared to the perforation friction.

2.2. Governing equations

The typical fracturing mathematical model should couple various processes, including rock deformation and fluid flow in the formation, fracture initiation and propagation, and flux proportioning between multi-cluster fractures. Besides the above-mentioned processes, the plugging behavior and flux re-proportioning process after diversion are extremely important during ITPF (Chen et al., 2020b). The plugging process of multi-cluster fractures in a horizontal well during ITPF is shown in Fig. 1. The diverters in the wellbore will flow with the fracturing fluid at the diverting time, and then plug the perforations of fractures in the over-developed zones (such as HF1 and HF3 in Fig. 1). After diversion, the subsequent fracturing fluid will be forced to flow into the under-developed zones (such as HF2 in Fig. 1), and then the under-developed will get effective propagation.

2.2.1. Rock deformation and fluid flow

Based on the principle of virtual work, the equilibrium equation for the solid skeleton in the porous media in the current configuration is (Zhang et al., 2010):

$$\int_V \left(\overline{\boldsymbol{\sigma}} - p_w \mathbf{I}\right)\delta\boldsymbol{\varepsilon} \mathrm{d}V = \int_S \mathbf{t}\cdot\delta\mathbf{v}\mathrm{d}S + \int_V \mathbf{f}\cdot\delta\mathbf{v}\mathrm{d}V \tag{1}$$

where $\overline{\boldsymbol{\sigma}}$ is the matrix of effective stress, Pa; p_w is the pore pressure in the rock matrix, Pa; $\mathbf{I}$ is the identity matrix, dimensionless; $\delta\boldsymbol{\varepsilon}$ is the matrix of virtual strain rate, s^{-1}; $\mathbf{t}$ is the surface traction vector per unit area, N/m^2; $\delta\mathbf{v}$ is the matrix of virtual velocity, m/s; $\mathbf{f}$ is the body force vector per unit volume, N/m^3.

The continuity equation of the fracturing fluid in the rock matrix can be written as (Wang et al., 2020b; Yu et al., 2019):

$$\frac{1}{J}\frac{\partial}{\partial t}(J\rho_w n_w) + \frac{\partial}{\partial \mathbf{X}}\cdot(\rho_w n_w \mathbf{v}_w) = 0 \tag{2}$$

where J is the volume change ratio of the porous media, dimensionless; t is the time, s; $\mathbf{v}_w$ is the fluid seepage flow velocity, m/s; n_w is the void ratio, dimensionless; ρ_w is the density of the injection fluid, kg/m^3; $\mathbf{X}$ is the spatial vector, m.

The fracturing fluid flow in the porous media will obey Darcy's law, and it is generally written as (Zhang et al., 2010):

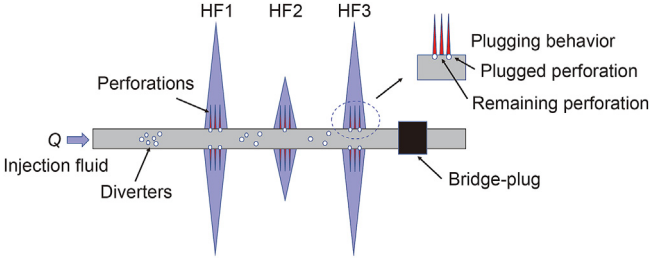

Fig. 1. The plugging process of multi-fracture during ITPF (HF: hydraulic fracture).

$$\mathbf{v}_w = -\frac{1}{n_w \mathbf{g}\rho_w}\mathbf{k}\cdot\left(\frac{\partial p_w}{\partial \mathbf{X}} - \rho_w \mathbf{g}\right) \tag{3}$$

where $\mathbf{g}$ is the gravity vector, m/s^2; $\mathbf{k}$ is the matrix permeability of the porous media, m/s.

2.2.2. Fracture initiation and propagation

The fracturing processes will be simulated using the cohesive zone element, which adopts the traction-separation law to characterize the constitutive relationship at the fracture tip, which avoids the stress singularity at the fracture tip based on the linear elastic fracture mechanics (LEFM). In general, the damage of a cohesive element undergoes three processes: damage initiation, damage evolution, and fracture generation.

Damage initiates once the total nominal stress ratios reach one. The quadratic nominal stress criterion is used as fracture initiation criteria (Simulia, 2019):

$$\left\{\frac{\langle t_n\rangle}{t_n^0}\right\}^2 + \left\{\frac{\langle t_{s1}\rangle}{t_{s1}^0}\right\}^2 + \left\{\frac{\langle t_{s2}\rangle}{t_{s2}^0}\right\}^2 = 1 \tag{4}$$

where t_n, t_{s1}, t_{s2} is the real nominal stress in the normal, the first and second shear nominal directions, Pa; t_n^0, t_{s1}^0, t_{s2}^0 is the peak nominal stress purely in the normal, the first and the second shear direction, Pa; $\langle\rangle$ is the Macaulay bracket.

Once the cohesive element meets the fracture initiation criterion, the stiffness of the cohesive element will degrade. The damage evolution equation describes the stiffness degradation rate. The degradation stress components of the traction-separation model are described by the following equations (Guo et al., 2017):

$$\begin{aligned} t_n &= \begin{cases} (1-D)\bar{t}_n, & \bar{t}_n \geq 0 \\ \bar{t}_n, & \bar{t}_n < 0 \end{cases} \\ t_{s1} &= (1-D)\bar{t}_{s1} \\ t_{s2} &= (1-D)\bar{t}_{s2} \end{aligned} \tag{5}$$

where $\bar{t}_n$, $\bar{t}_{s1}$ and $\bar{t}_{s2}$ are the predicted nominal stress in the normal, the first and second shear nominal directions through the bilinear traction-separation model for the current strains without damage, Pa; D is the damage factor, dimensionless. And it's expressed as (Simulia, 2019):

$$D = \frac{\delta_m^f\left(\delta_m^{max} - \delta_m^0\right)}{\delta_m^{max}\left(\delta_m^f - \delta_m^0\right)} \tag{6}$$

where δ_m^0, δ_m^f, δ_m^{max} are the displacement at the stage of fracture initiation, fracture generation, and the maximum value during the loading history, m.

2.2.3. Fluid flow within the fracture

Once the fracture is formed, the fluid will flow within the fracture in the two flow directions. One is the tangential flow process along the fracture direction and the other is the normal flow process across the fracture. Fig. 2 shows the two fluid-flow processes within the cohesive element.

Flow behavior along the fracture direction can be described by Poiseuille's law, and the flow equation is governed by (Simulia, 2019):

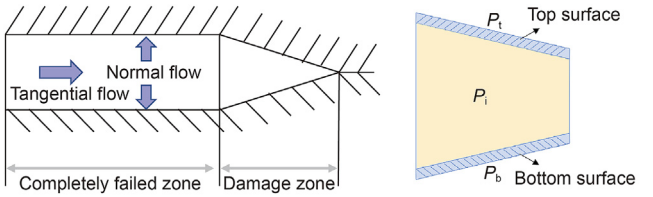

(a) Flow in the cohesive element **(b)** Normal leak-off flow process

Fig. 2. Sketch of fluid flow processes in the cohesive element.

$$q = -\frac{w^3}{12\mu}\nabla p \tag{7}$$

where q is the mass flowrate along the fracture direction, m^2/s; w is the fracture opening, m; μ is the viscosity of fracturing fluid, cP; p is the fluid pressure within the fracture, Pa.

The leak-off flow process across the fracture in the cohesive element method is shown in Fig. 2b and defined as the following equation, which is also the common choice in the FEM simulations (Shin and Sharma, 2014; Li et al., 2021; Guo et al., 2017):

$$\begin{cases} q_t = c_t(p_i - p_t) \\ q_b = c_b(p_i - p_b) \end{cases} \tag{8}$$

where c_t, c_b is the leak-off coefficient into the top and bottom fracture surfaces, respectively, m/s/Pa; p_i, p_t, p_b are the pore pressures within the fracture, top fracture surface, and bottom fracture surface, respectively, Pa; q_t, q_b are the normal flowrates into the top and bottom fracture surfaces, m/s.

Besides, the fluid within the fracture also satisfies the continuity equation (Simulia, 2019):

$$\frac{\partial w}{\partial t} + \nabla \cdot q + (q_t + q_b) = Q(t)\delta(x, y) \tag{9}$$

where $Q(t)$ is the injection rate at a known location, m/s; $\delta(x, y)$ is Kronecker's delta function.

2.2.4. The flux partitioning model before or after perforation plugging

The fracturing fluid in the horizontal wellbore will flow through the perforation clusters and enter each cluster of fractures. The flux proportioning between multi-cluster fractures mainly depends on the perforation friction through each fracture. The relationship between the perforation friction and the flowrates is described as follows (Crump and Conway, 1988):

$$\Delta p^i_{\text{fric}} = \alpha_{p,i} Q_i^2 \tag{10}$$

$$\alpha_{p,i} = 0.807249 \frac{\rho}{N_{p,i}^2 D_{p,i}^4 C^2} \tag{11}$$

where i is the number of fracture clusters, dimensionless; Δp^i_{fric} is the perforation friction through the ith fracture, Pa; Q_i is the fluid flowrate of the ith fracture, m^3/s; ρ is the fluid density, kg/m^3; $N_{p,i}$ is the perforation number of the ith fracture before diversion, dimensionless; $D_{p,i}$ is the perforation diameter of the ith fracture, m; C is a dimensionless discharge coefficient ranging between 0.56 (before erosion) and 0.90 (after erosion).

The pipe fluid connector element (FPCE) with two pore-pressure nodes is adopted to simulate the perforation friction and the flux proportioning between multi-cluster fractures in our study. The fluid will inflow in one pore-pressure node and outflow to another pore-pressure node, while a pressure drop associated with the flowrate will be produced, as shown in Fig. 3. The pressure drop through this element is based on the Bernoulli's equation. This equation could also describe the flow process through the perforation channel, which is a common choice in the previous study (Crump and Conway, 1988; Cramer et al., 2020). Its expression is

$$\Delta p = p_1 - p_2 = \frac{K}{2}\rho v_i^2 \tag{12}$$

where K is the loss term in the fluid pipe connector element, dimensionless; v_i is the fluid velocity through the ith fracture in the wellbore, m/s; Δp is the pressure drop through the fluid pipe connector element, Pa; p_1 and p_2 are the pore pressure at the inflow node and outflow node, respectively, Pa.

In addition, multiple FPCEs could be combined into a pipe network to simulate the flow process between multi-cluster fractures (i.e. three fractures in Fig. 4), the flowrates and pressures of this pipe network will satisfy the following equations:

$$Q_{\text{total}} = \sum_i^n Q_i \quad i = 1,\ 2,\ 3,\ \cdots,\ n \tag{13}$$

$$P_{\text{wellbore}} = P_{\text{out},i} + P_{\text{pf},i} \quad i = 1,\ 2,\ 3,\ \cdots,\ n \tag{14}$$

where Q_{total} is the total flowrate in the wellbore, m^3/s; Q_i is the flowrate of the ith fracture, m^3/s; $P_{\text{out},i}$ is the pore pressure of the outflow node in the ith fracture, m^3/s; P_{wellbore} is the pore pressure in the wellbore, Pa; $P_{\text{pf},i}$ is the perforation friction of the ith fracture, Pa.

The pressure loss coefficient K is different before and after perforation plugging in Eq. (12) due to the perforation plugging behavior. Therefore, the user subroutine UFLUIDCONNECTORLOSS based on the finite analysis code is developed to activate different loss coefficients K to satisfy the perforation friction model and dynamic plugging model, respectively.

2.2.4.1. Before perforation plugging. To accurately simulate the relationship between the pressure friction and the flowrates of the perforations in Eq. (10), the loss term K before perforation plugging could be modified to the following equation:

$$K_{\text{per,b}} = \frac{2\alpha_p A^2}{\rho} \tag{15}$$

where $K_{\text{per,b}}$ is the perforation loss term before perforation plugging, dimensionless; A is the horizontal wellbore cross-sectional area, m^2; α_p is the perforation coefficient before perforation plugging, shown in Eq. (11).

2.2.4.2. After perforation plugging. As mentioned earlier in Fig. 1, some perforations of multi-cluster fractures will be plugged by diverters at the diverting time. The number of perforations in each fracture would be changed after perforation plugging. The plugging equation will be also coded and accomplished using the subroutine UFLUIDCONNECTORLOSS. And this subroutine would be activated at the diverting time to achieve the perforation plugging behavior.

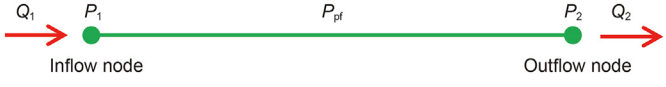

Fig. 3. Sketch of fluid flow within fluid pipe connector element.

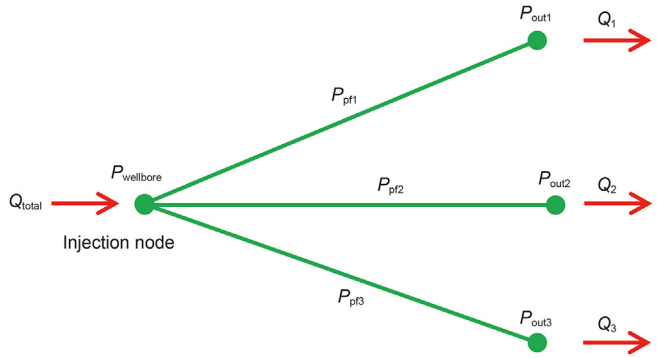

Fig. 4. Sketch of fluid flow within three FPC3D2 elements.

In this subroutine, the loss term K after perforation plugging could be modified to the following equation:

$$K_{\mathrm{per,a}} = \frac{2\alpha_{\mathrm{r}}A^2}{\rho} \tag{16}$$

where $K_{\mathrm{per,a}}$ is the perforation loss term after perforation plugging, dimensionless; α_{r} is the perforation coefficient after perforation plugging, dimensionless.

According to Eq. (11), the perforation coefficient α_{r} after perforation plugging is determined as:

$$\alpha_{\mathrm{r},i} = 0.807249\frac{\rho}{N_{\mathrm{r},i}^2 D_{\mathrm{p},i}^4 C^2} \tag{17}$$

where $N_{\mathrm{r},i}$ is the number of remaining perforations in the ith fracture after plugging, dimensionless;

To calculate the remaining perforation number after plugging, we adopted one reasonable assumption from Chen et al. (2020b) that the diverters will be uniformly distributed in the fracturing fluid (Chen et al., 2020b). The number of diverters in one fracture will be determined by the product of the flowrate ratio of the fracture and the total number of diverters (shown as Eq. (17)). The flowrate ratio means the ratio of flowrate in one fracture to the total flowrate in the horizontal wellbore. Hence, the location of diverters in each fracture will be determined by the following equation (Chen et al., 2020b):

$$N_{\mathrm{plug},i} = \left[N_{\mathrm{d}}\frac{Q_i}{Q_{\mathrm{total}}}\right] \tag{18}$$

After plugging, the remaining perforations of each fracture after plugging can be determined as:

$$N_{\mathrm{r},i} = N_{\mathrm{p},i} - N_{\mathrm{plug},i}, \quad i = 1,\ 2,\ \ldots,\ n \tag{19}$$

where N_{d} is the total number of injected diverters at the plugging time; $N_{\mathrm{plug},i}$ is the number of plugged perforations of the ith fracture at the diverting time; $[\cdot]$ is the least integer function;

3. Model validation

The cohesive zone method (CZM) has been widely applied and verified in the hydraulic fracturing simulation. For example, Chen et al. (2009) verified the cohesive element with the KGD analytical solution in the toughness-dominated regime. Subsequently, Chen et al. (2012) verified the cohesive element with the analytical solution in the viscosity-dominated regime. Taleghani et al. (2018) also proved the accuracy of cohesive element numerical simulation and laboratory experiments. Hence, the verification of the cohesive element will be not repeated in this paper.

In this part, the accuracy of the flux partitioning model considering perforation plugging based on the fluid pipe element and its subroutine will be verified with the analytical model. The validation work includes three aspects: firstly, flux partitioning test in the hydraulic fracturing; secondly, plugging behavior when injecting diverters; thirdly, fluid re-partitioning test after plugging. In this section, three fluid pipe connector elements were created to realize the dynamic flux partition at the diverting time. As shown in Fig. 4, the left node of this model was a common injection node with pressure P_{wellbore} and the total injection rate was 6 m^3/min. Three right nodes were outflow nodes and their pressures were P_{out1}, P_{out2}, and P_{out3}, respectively. The perforations of three fractures have the same parameters: $N_{\mathrm{p},1} = N_{\mathrm{p},2} = N_{\mathrm{p},3} = 15$, $D_{\mathrm{p}} = 0.01$ m, $C = 0.60$, $\rho = 1000$ kg/m^3. The specific validation consists of three main processes: (1) flux partitioning process (0–12 s), P_{out1} and P_{out3} were both 4 MPa, and P_{out2} changed from 6 to 2 MPa with a cosine wave; (2) plugging process (12 s), twenty diverters were injected to plug the perforations, and the flux partitioning model after perforation plugging will be activated to simulate the plugging behavior at the diverting time; (3) fluid re-partitioning process after diversion (12–20 s): P_{out1} and P_{out3} were both 4 MPa, and P_{out2} was 2 MPa. In this verification, the pressure boundary conditions in these three right nodes were known variables and they are given in Fig. 5a.

The flowrate and the perforation friction of each fluid pipe element are the most concerned unknown information for the multiple fracture propagation. Therefore, the values of P_{wellbore}, P_{pf1}, P_{pf2}, P_{pf3}, Q_1, Q_2, Q_3 were considered as the unknown variables and

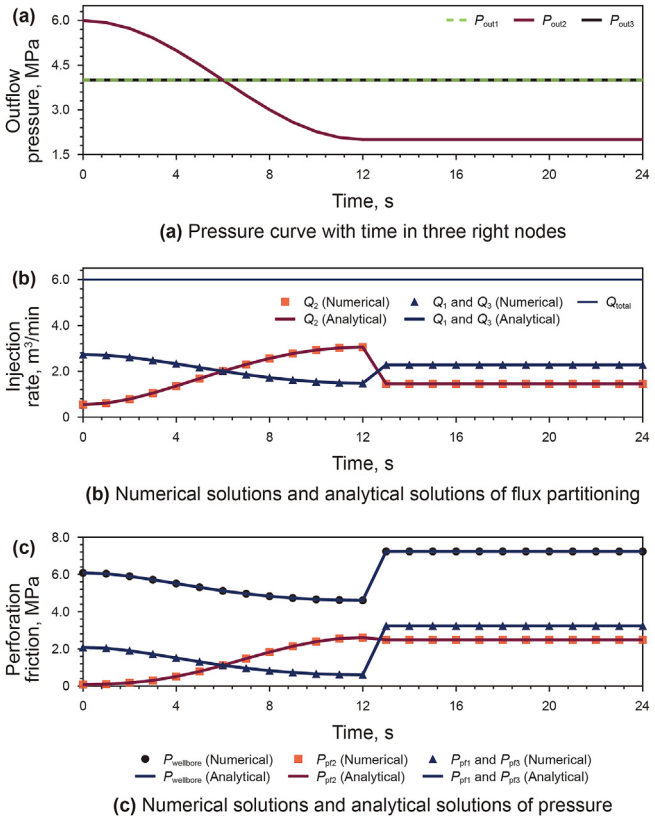

Fig. 5. Validation of flux partitioning and plugging behavior in the FPCE element and the subroutine (three processes are included: 1. Flux partitioning process (0–12 s); 2. Plugging process (12 s); 3. Fluid re-partitioning process after plugging (12–20 s)).

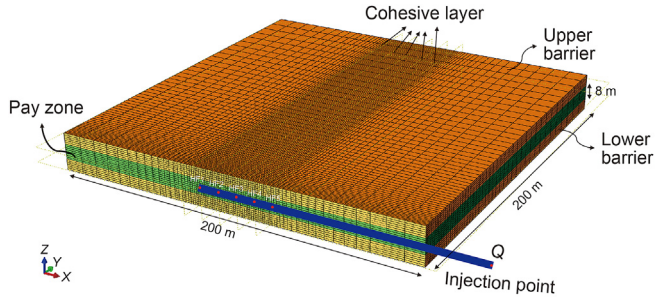

Fig. 6. Three-dimensional reservoir model.

need to be calculated by the fluid pipe element. These variables will be verified with the analytical solutions. Fig. 5b and c show the numerical solutions and analytical solutions of the flux partitioning and perforation pressure. These two figures showed there was a good agreement in the simulation results and analytical solutions in the three processes. Therefore, our flux partitioning model can provide accurate results for the flux partitioning process and the plugging behavior.

4. Results

4.1. Model description

The three-dimensional finite element model was established as shown in Fig. 6 and its size was 200 m × 200 m × 20 m in the *x*, *y*, and *z* directions, respectively. The total model was divided into the surrounding rock and target model. Coarse mesh size was used in the surrounding rock to eliminate the influence of boundaries, and a fine mesh size was used in the target model to capture fracture propagation (Fig. 6). However, extremely fine mesh sizes can dramatically increase the computational cost, while coarse meshes can not obtain the fracture geometry. Hence, to reduce computational costs and meanwhile maintain geometry accuracy, the grid size of 1 m × 1 m × 1 m of cohesive elements has been chosen in the engineering-scale model according to the grid sensitivity results from Li et al. (2020).

Due to the symmetry of the full model, a half model will be used to simulate the fracture propagation behavior because of its low computational cost. In this model, the height of the pay zone was 8 m, and the height of the upper and lower barriers was 6 m. A horizontal wellbore was distributed in the center of the pay zone, and five-cluster fractures were symmetrically distributed in the center position, named HF1, HF2, HF3, HF4, and HF5. The fracturing spacing was 10 m. The injection flowrate at the injection point was designed as 12 m^3/min, and then the fracturing fluid in the wellbore was automatically distributed to five-cluster fractures by fluid pipe elements. This model contained 86,700 elements in total, including 81,600 C3D8P elements (three-dimensional continuum elements with eight pore-pressure nodes), which represent the rock matrix; 5100 COH3D8P elements (three-dimensional cohesive elements with eight pore-pressure nodes), which represent hydraulic fracture; five FPC3D2 elements (three-dimensional fluid pipe connector elements with two pore-pressure nodes), which represent five perforation clusters. Table 1 shows the basic parameters.

4.2. Comparison of the base case and the diversion case

In this section, the diversion case of five-cluster fractures was compared with the base case. In the base case, no diverters were injected. While in the diversion case, forty diverters were injected to achieve the perforation plugging at half of the total fracturing time, i.e. six hundred seconds. Other parameters were the same as in Table 1. We will analyze the fracture propagation geometry, wellbore pressure, flowrate, and fluid volume of each fracture in two cases.

Figs. 7 and 8 show the 3D geometries of five-cluster fractures in the base case and the diversion case. From Fig. 7, the phenomenon of uneven propagation became more and more serious with the increase in injection time in the base case. Specifically, the fracture lengths of the five clusters were almost the same at the time of 100 s. While at the time of 1200 s, the ratio of the longest fracture length to the shortest fracture length was 9.5. From Fig. 8, the non-uniform propagation in the diversion case was completely consistent with that of the base case before the diverting time. However, the non-uniform phenomenon has been improved and the ratio of

Table 1
Basic parameters of the model.

Categories	Parameters	Value	
		Pay zone	Barrier zone
Rock properties	Young's Modulus, GPa	45	35
	Poisson's ratio	0.20	0.23
	Permeability coefficient, m/s	1e-6	1e-8
	Porosity, %	10	6
	Pore pressure, MPa	45	45
	In-situ stress, MPa	50/62/65	55/62/65
Fracture properties	Initial damage stress, MPa	4	6
	Tension fracture energy, J/m^2	1000	1500
	Shear fracture energy, J/m^2	2000	3000
	Initial elastic cohesive stiffness, GPa/m	1200	1200
	Leak-off coefficient, m/(Pa s)	1e-13	1e-14
Fluid parameters	Fluid viscosity, mPa s	1	
	Total injection time, s	1200	
	Injection rate, m^3/min	12	
	Fracturing fluid density, kg/m^3	1000	
Perforation parameters	Perforation diameter, mm	10	
	Dimensionless discharge coefficient	0.60	
	Perforation number per cluster	16	
	Total number of in-stage perforation	80	
Plugging parameters	Number of diverters	40	
	Diverting time, s	600	
	Injection frequency	1	

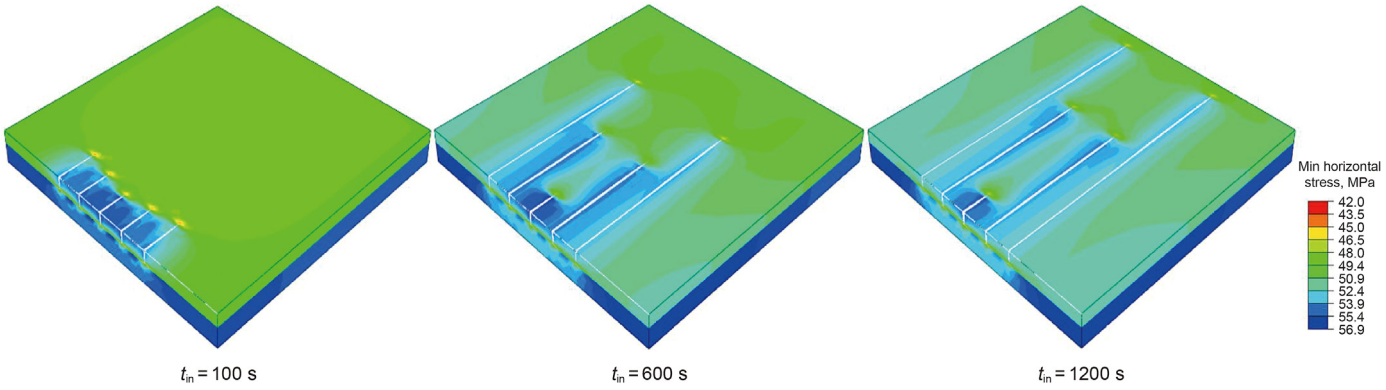

Fig. 7. Fracture propagation geometries of the base case.

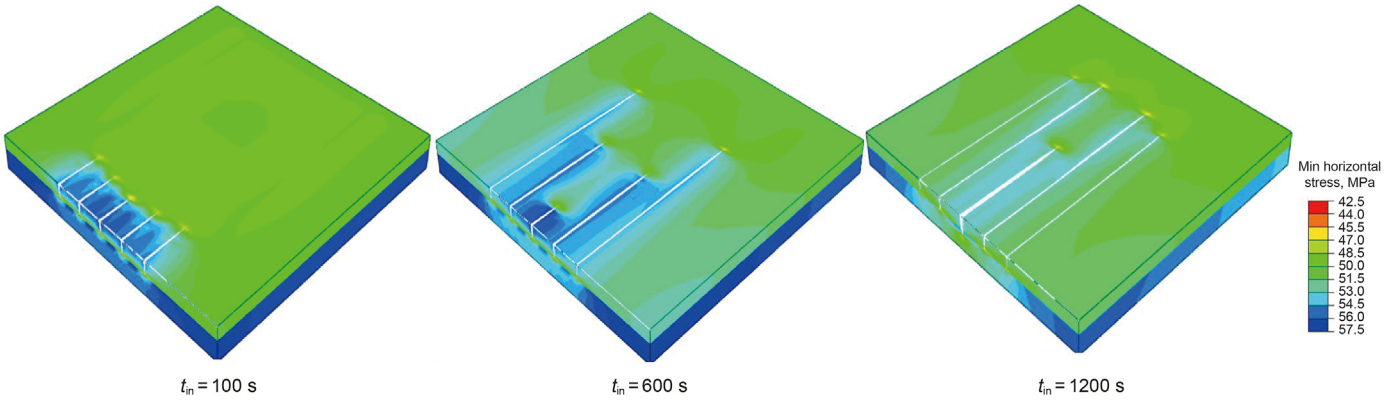

Fig. 8. Fracture propagation geometries of the diversion case.

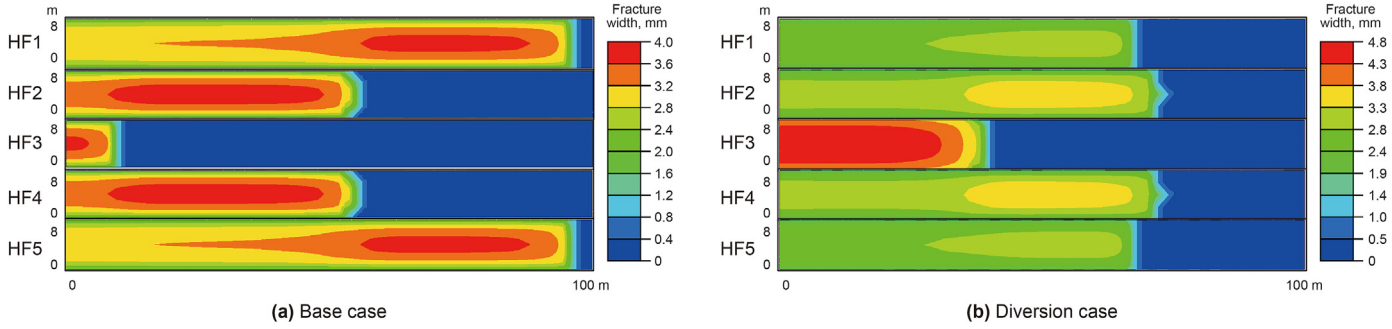

Fig. 9. Fracture profiles of the base case and the diversion case.

the longest fracture length to the shortest fracture length was only 1.8 when the full fracturing process was over.

To observe final fracture propagation geometries directly, the fracture profiles of two cases were extracted for further analysis (Fig. 9). In Fig. 9a, a good symmetry could be found in the fracture propagation geometries, and the length of side fractures (HF1 & HF5), sub-side fractures (HF2 & HF4) and central fracture (HF3) were 95, 56, and 10 m, respectively. While in the diversion case, they were 68, 74, and 40 m, respectively. Although the middle fractures were injected continuously fluid by plugging the other fractures during ITPF, the middle fractures were still hard to propagate forward and then produced a larger fracture width. This was because the middle fractures usually have greater local stress and a higher propagation resistance due to the stress shadow. The standard deviation is a common measurement basis for the degree of discrete distribution of statistical data, and its calculation formula is Eq. (20). Usually, the larger the value of standard deviation, the more uneven the sample data. On the contrary, the smaller the value of standard deviation, the more uniform the sample data.

$$\sigma = \sqrt{\frac{1}{N}\sum_{i=1}^{N}(x_i - \overline{x})^2} \tag{20}$$

where σ is the standard deviation; N is the number of sample data; x_i is the ith sample value; $\overline{x}$ is the average value of N samples.

In this study, the standard deviation of the fracture length was used to represent the uniformity of multi-fracs length. The standard deviation in the base case and the diversion case were 35.18 and

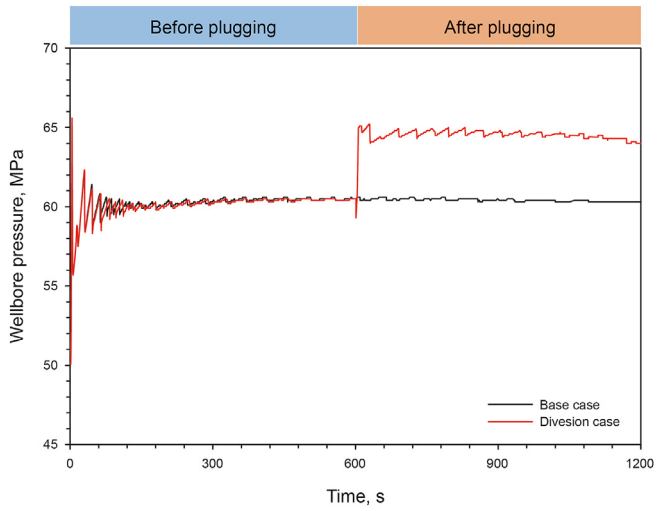

Fig. 10. Wellbore pressure changes of the diversion case and the base case.

14.18, respectively, which also indicates that the diversion case had a more uniform fracture length than those in the base case.

The wellbore pressure curves in the base case and the diversion case are shown in Fig. 10. From this figure, we can conclude that the perforation plugging behavior in the diversion case usually can be characterized by a sudden wellbore pressure rise compared to the pressure curve in the base case. Specifically, the wellbore pressure in the diversion case sharply rose to 65.3 MPa at the diverting time, rising by 4.9 MPa while the wellbore pressure of the base case was maintained at 60.4 MPa after hydraulic fractures were initiated.

As shown in Fig. 11, compared to the base case, perforation plugging led to a dramatic flux re-proportioning of fractures at the diverting time in the diversion case, which could explain the uniform propagation of the fractures in the diversion case. From Fig. 11a, due to the strong competitive propagation between fractures in early fracturing, the pressure and the flowrates in each fracture will show some fluctuations. After a certain time (300 s), the flowrate of side fractures, sub-side fractures, and center fracture were maintained at 3.5, 2.3, and 0.4 m^3/min respectively. In the diversion case, the flowrates changed drastically at the diverting

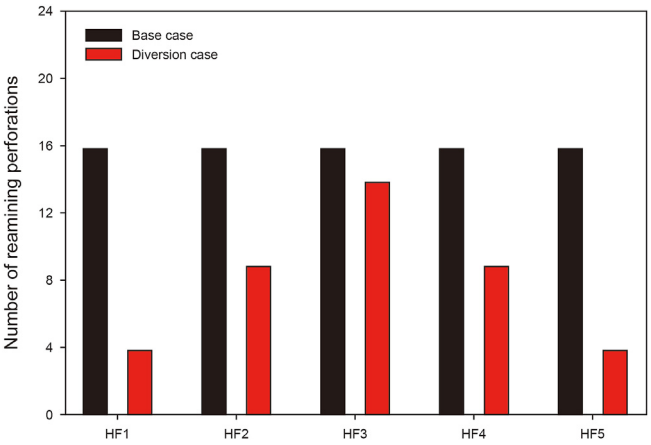

Fig. 12. Perforation numbers of each fracture in the base case and the diversion case.

time and the flowrates of side fractures were rapidly reduced from 3.5 to 1.4 m^3/min; the flowrate of the center fracture increased from 0.3 to 3.8 m^3/min. According to the flowrates at the diverting time, the number of plugged perforations in each fracture has been calculated through Eq. (18) and the number of remaining perforations was four, nine, fourteen, nine, and four, respectively (Fig. 12). Hence, the mechanism of perforation plugging lies in that the perforation plugging changes the original distribution of the number of perforations, thus changing the flux partitioning after the diverting time, which balances the fluid volume and fracture propagation of each fracture.

Fig. 13 shows the fluid volume proportion of each fracture in the base case and the diversion case. In the base case, the average fluid volume partition of the side fractures, sub-side fractures, and center fracture were 28.2%, 19.5%, and 4.6%, respectively. The standard deviation of fluid volume in the base case was 9.67. However, the average fluid volume partition in the diversion case was more uniform and they were 21.7%, 20.5%, and 15.5%, respectively. Compared to the based case, the standard deviation of fluid volume in the diversion case was just 0.82, which was only 8.48% of that in the base case. The fluid volume proportion indicates perforation plugging also improves the uniformity of fluid volume

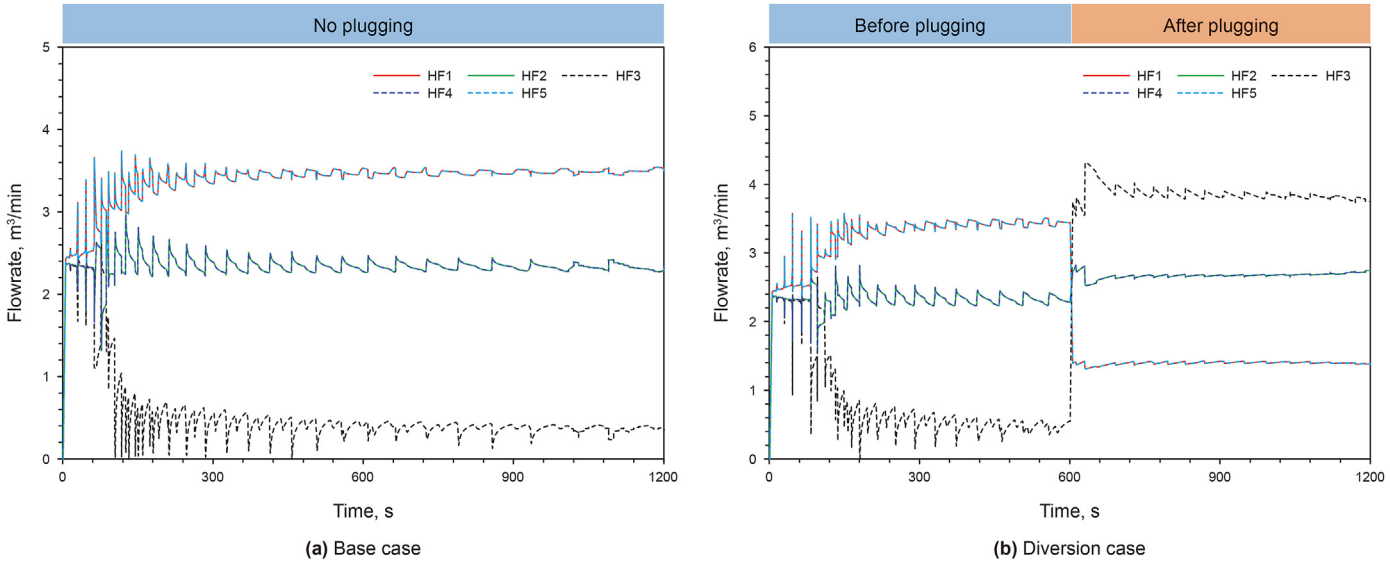

Fig. 11. The flowrate of each fracture in the base case and the diversion case.

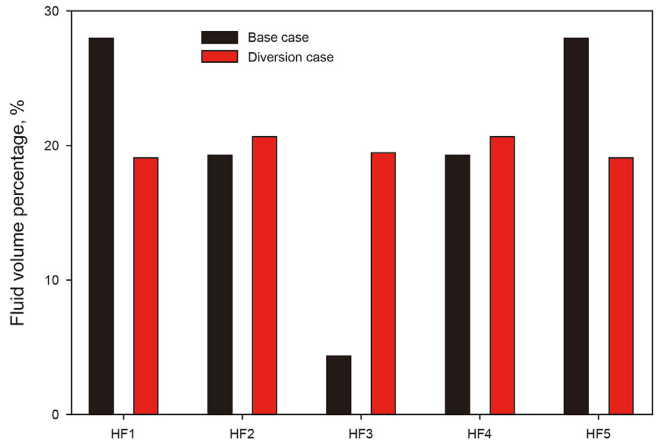

Fig. 13. Fluid volume percentages of each fracture in the base case and the diversion case.

proportion of each fracture, which is consistent with fracture geometries in Fig. 9.

4.3. Effect of the number of diverters

The number of diverters is one of the most important parameters and directly determines the plugging effectiveness during ITPF. In this section, the effect of the number of diverters on the propagation of multi-cluster fractures will be investigated. The number of diverters will be changed to eight, twenty-four, forty, and fifty-six respectively, which is equivalent to 10%, 30%, 50%, and 70% of the total number of perforations in one stage (N_{pt}) while other parameters remain the same in Table 1.

Fig. 14 shows the fracture profiles with the different numbers of diverters. From Fig. 14a–d, the uniformity of fracture length became higher when the number of diverters increased from 10% N_{pt} to 70%N_{pt}, and meanwhile, the total fracture length also became larger using more diverters. Specifically, when the number of diverters increased from 10%N_{pt} to 70%N_{pt}, the total length of five fractures increased from 308 to 352 m, increasing by 14.29%. Meanwhile, the standard deviation of fracture length of five fractures decreased from 29.41 to 8.76, reducing by 70.21%.

Fig. 15 shows the wellbore pressure curves with the different number of diverters. The more the number of diverters injected, the higher the wellbore pressure rises at the diverting time. Particularly, the wellbore pressure rises in these four cases were 0.4, 1.5, 4.9, and 15.3 MPa, respectively. Although the perforation plugging behavior increases the fluid pressure in the wellbore, which facilitates the uniform propagation of multiple fractures, however, when the wellbore pressure was too high, such as 15.3 MPa, the risk to wellbore integrity or safety increases dramatically. Therefore, selecting the right number of diverters should not only fully consider the uniformity of the fracture length, but also the pressure-bearing condition of the wellbore, otherwise, the stimulation operation by perforation plugging may be failed.

Fig. 16 shows the fluid volume distribution of each fracture in four cases. From this figure, the fluid volume distribution changed from a “concave” shape to a “convex” shape. The concave shape means that the side fractures receive more fluid, while the center fracture receives less fluid. On the contrary, the convex shape means that the side fractures receive less fluid, while the center fracture receives more fluid. The fluid distribution of side fractures, sub-side fractures, and center fracture with eight diverters were 26.78%, 18.7%, and 8.71%, respectively, while the fluid distribution with fifty-six diverters was 13.71%, 20.27%, and 32.03%, respectively. Meanwhile, the standard deviations of fluid volume have also been calculated with the different numbers of diverters and they were 7.45, 3.93, 0.82, and 7.49. Therefore, when the number of diverters was 50%N_{pt}, the standard deviation of fluid distribution was only 0.82, which was lower than the cases of 10%N_{pt}, 30%N_{pt} and 70%N_{pt}. Comprehensively considering pressure rise and fluid distribution, the number of diverters was recommended to be 50% of the total number of perforations.

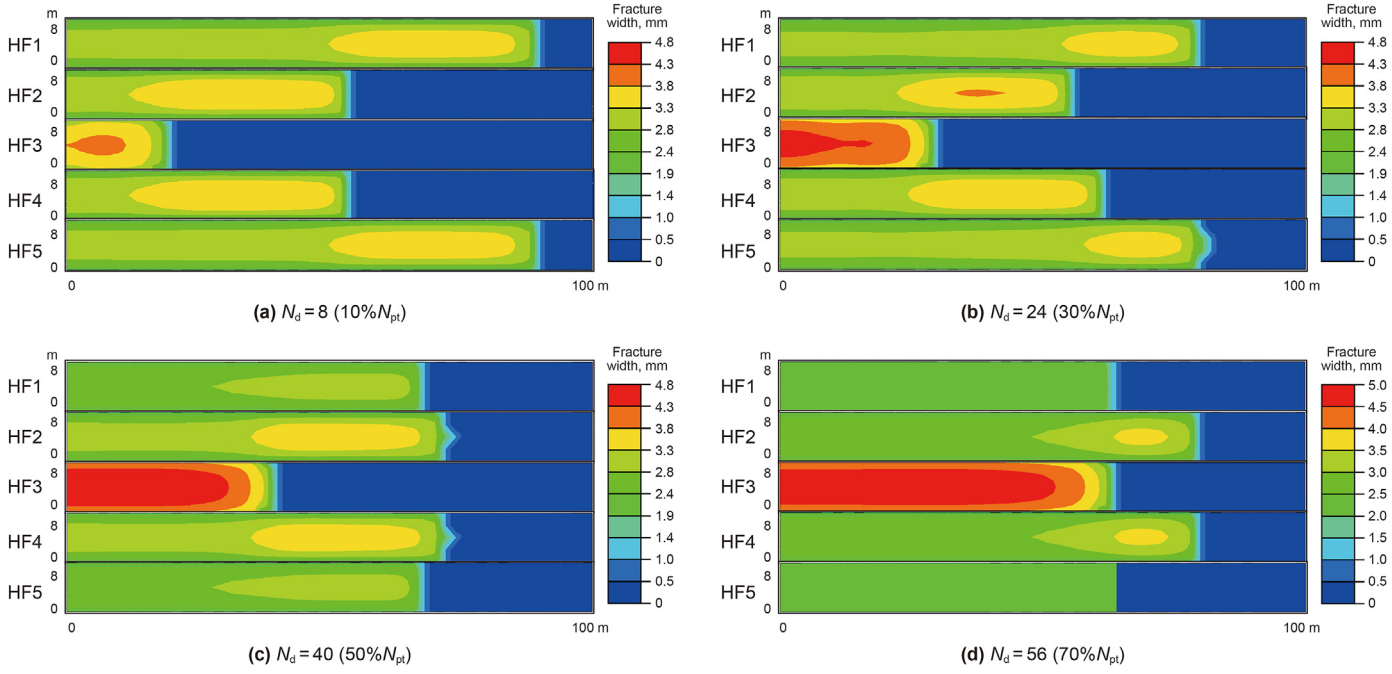

Fig. 14. Fracture profiles with different numbers of diverters (N_{pt}: the total number of perforations in one stage; N_d: the number of diverters).

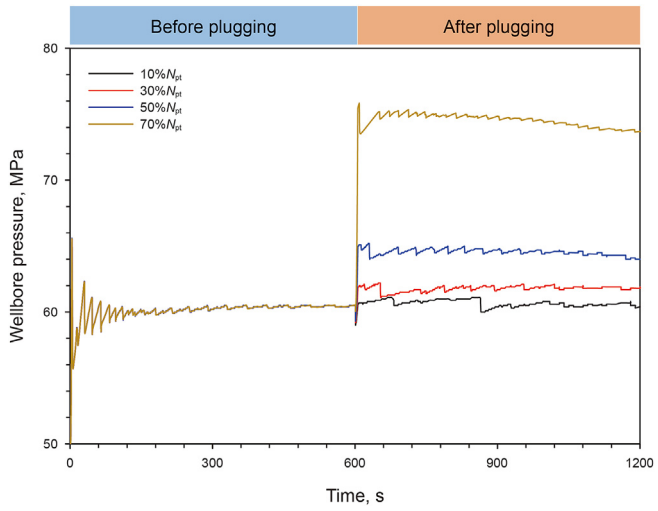

Fig. 15. Wellbore pressures with different temporary plugging balls.

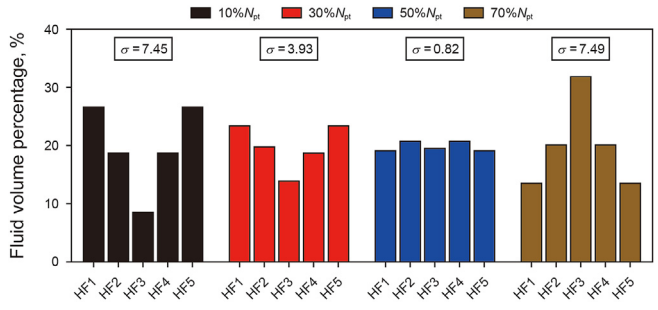

Fig. 16. Fluid volume percentages of each fracture with the different numbers of diverters.

4.4. Effect of the diverting timing

The diverting timing is the time when diverters are injected during ITPF, which determines when the over-treated fractures are plugged and also could affect the final fracture geometries. In this section, forty diverters were injected at different diverting timing (240, 480, 600, 840 s) to investigate the effect of the diverting timing on the uniformity of fracture propagation.

Fig. 17 shows the fracture profiles of the cases with different diverting timing. As shown in Fig. 17 the earlier the diverting timing was, the longer the length of the middle fracture was; the later the diverting timing was, the longer the lengths of the side fractures were. Specifically, when diverting timing was 240 s (20% of the total fracturing time, t_{ft}), the length of the middle or sub-middle fractures (HF2, HF3, and HF4) were 78, 56, and 78 m, which was larger than that of the side fractures (48 m). While the diverting timing was 840 s (70%t_{ft}), the lengths of the side fractures (HF1 & HF5) were 80 m, which was larger than that of the middle fractures. This was because the perforations of side fractures have been prematurely plugged and the side fractures have not been effectively propagated when the diverting timing was earlier, i.e. 20%t_{ft}. When the diverting timing was later, i.e. 70%t_{ft}, a large amount of fracturing fluid flowed into the side fractures, while subsequent fluid flowing into the middle fracture was too little to complete uniform propagation. The standard deviations of these four cases were 15.32, 10.71, 14.18, and 21.38, respectively.

Fig. 18 shows the wellbore pressure curves of the cases with different diverting timing. From this figure, it can be seen that a sharp wellbore pressure increase occurred only at the diverting timing. Besides, although the diverting timing was different, the plugging pressure rise was the same, about 4.9 MPa. The number of injected diverters in these four cases was the same and hence the wellbore pressure at the different diverting timing has the same rise pressure.

Fig. 19 shows the fluid volume of each fracture in four cases at different diverting timing. Similar to fracture geometries, the

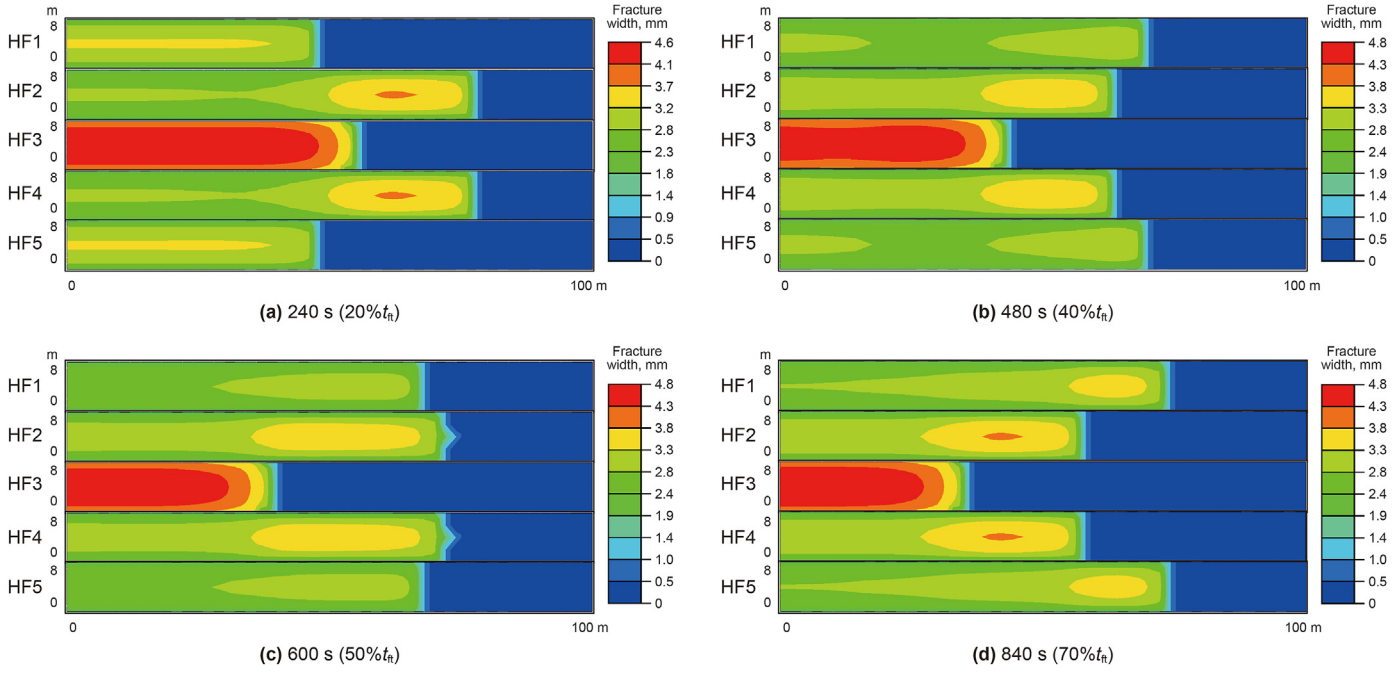

Fig. 17. Fracture profiles with different diverting timing (t_{ft}: the total fracturing time).

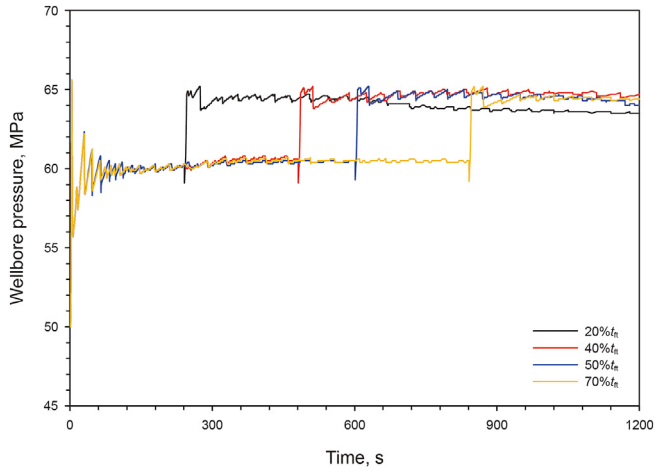

Fig. 18. Wellbore pressure at different diverting timing during ITPF (t_{ft}: the total fracturing time).

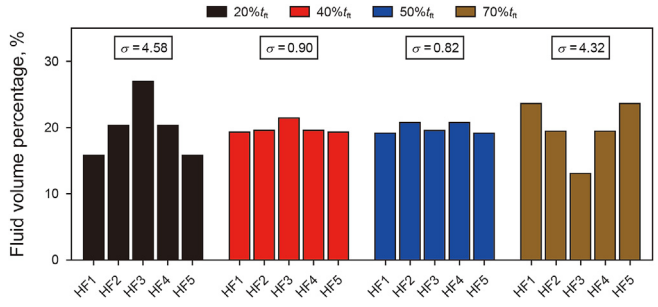

Fig. 19. Fluid volume percentages of each fracture at different diverting timing (t_{ft}: the total fracturing time).

earlier the diverting timing was, the more fluid volume of the middle fractures obtained. The later the diverting timing was, the less fluid volume of the side fractures obtained. The standard deviations of four cases at different diverting timing were 4.58, 0.90, 0.81, and 4.32 respectively. The values of standard deviation in the early-stage diversion case (20%t_{ft}) or the later-stage diversion case (70%t_{ft}) were larger than the values of the middle-stage diversion cases (40%t_{ft} or 50%t_{ft}). This indicates that the diverters should be injected at an appropriate timing, i.e. cases of injecting at 40%t_{ft} or 50%t_{ft}, whose standard deviations of the fluid distribution were only about 20% of standard deviations in the cases of injecting at 20%t_{ft} or 70%t_{ft}.

4.5. Effect of injection frequency with the same total number of diverters

Using the same total number of diverters, whether these diverters are injected once or multiple injection times is a very important discussion in the field operation design. In this section, forty diverters were injected once, twice, three times, and four times. The number of diverters injected each time was the total number of diverters divided by the injection frequencies as shown in Table 2.

Fig. 20 shows these fracture profiles in four cases. The standard deviations of fracture lengths in these four cases were 14.18, 15.62, 16.33, and 15.53, respectively. Although the values of standard deviations were relatively close, the results show that injecting all diverters once could have a more uniform fracture length than injecting multiple times. It should be pointed out that this conclusion was obtained under the conditions of the same total number of diverters and the average number of diverters. Subsequent research will further explore the influence of the different proportions of the number of diverters and diverting timing on the fracture propagation during multiple diversion times.

Fig. 21 shows wellbore pressure curves with different injection frequencies with the same total number of diverters. The wellbore pressure in the case with one injection frequency case has undergone a sharp rise (Fig. 21a), while the wellbore pressures in the cases with multiple injection frequencies have experienced multiple small pressure rises but the final rise of wellbore pressure was equal in all four cases (from Fig. 21b–d). The same final pressure was due to the same number of diverters in the whole ITPF process, which caused the same perforation friction to rise. Note that the case with a single injection could maintain a higher well-hole pressure for a longer period than the cases with multiple injections, which could further explain why the once injection case was more effective than others.

Fig. 22 shows the fluid volume percentage of each fracture with different injection frequencies. The fluid proportion of side fractures in the multiple injection frequencies slightly increased compared to that in the case with a single injection. The standard deviations of the fluid volume percentage with the injection frequency of one, two, three, and four were 0.82, 1.48, 1.88, and 1.72, respectively. The results show that multiple injection cases have a lower uniformity of fluid distribution than the case with a single injection. According to the values of standard deviation, the standard deviation of the once injection case was about 43.62%–55.41% of the other cases. As we mentioned earlier, the case with a single injection could last a longer period than the multiple injection case for the high wellhole pressure, which ensures a more effective and balanced fluid distribution in multiple fractures.

5. Discussion

The distribution of the fracture length and fluid injection volume are the two most critical parameters in the multi-fracture simultaneous propagation. To understand the uniformity of fracture length and fluid injection volume, the dimensionless parameters were defined and calculated to match the changes of different parameters, and its value is the ratio of variable parameters to the standard diversion case (the diverting timing is 600 s, the number of diverters is forty, the injection frequency of diversion is one).

Table 2
Cases with different injection frequencies using the same total number of diverters.

Injection frequency	First diversion		Second diversion		Third diversion		Fourth diversion		N_d
	Time, s	$N_{d,1}$	Time, s	$N_{d,2}$	Time, s	$N_{d,3}$	Time, s	$N_{d,4}$	
One	600	40	/	/	/	/	/	/	40
Two	360	20	720	20	/	/	/	/	40
Three	300	13	600	14	900	13	/	/	40
Four	240	10	480	10	720	10	960	10	40

($N_{d,i}$: the number of diverters in the ith diversion; N_d: the total number of diverters).

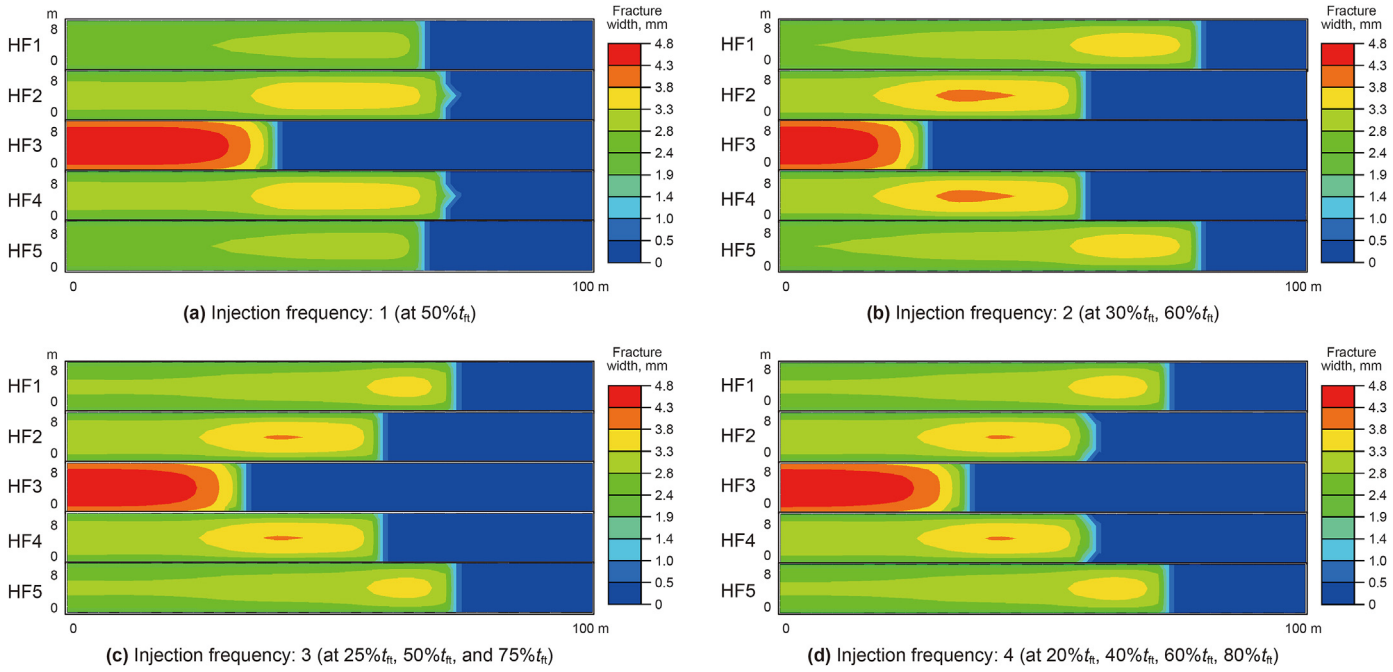

Fig. 20. Fracture profiles with different injection frequencies with the same total number of diverters (t_{ft}: the total fracturing time).

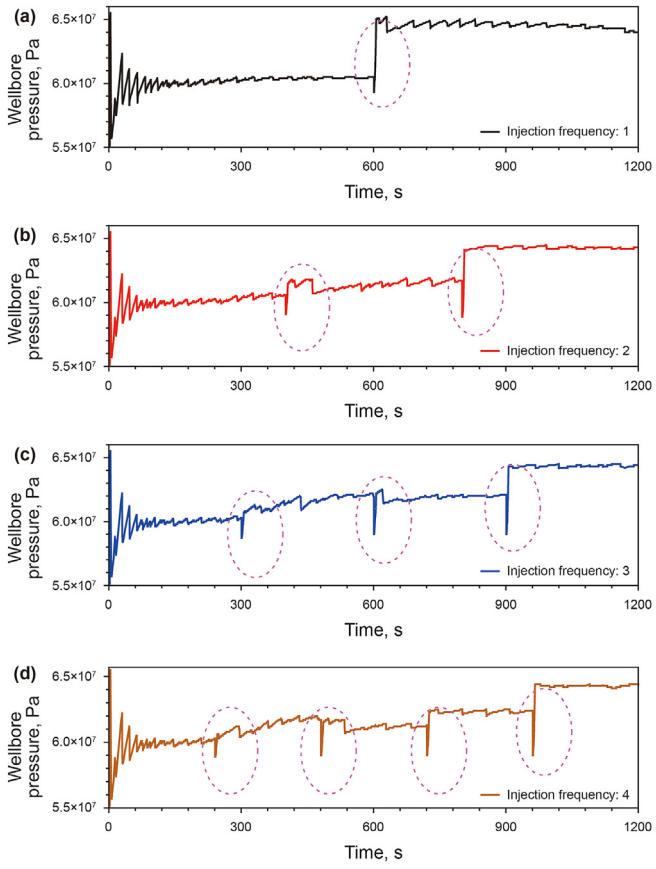

Fig. 21. Wellbore pressure with different injection frequencies with the same total number of diverters.

Fig. 23a and Fig. 23b show the variation of the standard deviation of the fracture length and fluid injection volume in each fracture under different dimensionless parameters.

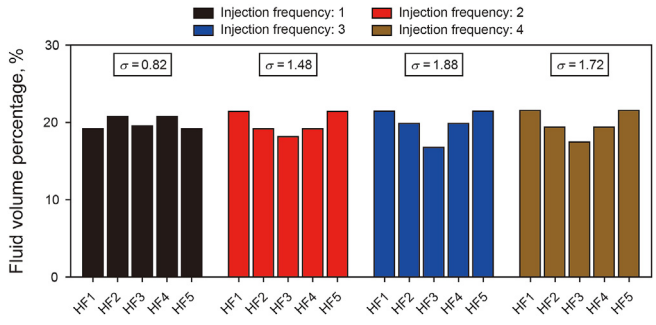

Fig. 22. Fluid volume percentages of each fracture with different injection frequencies with the same total number of diverters.

In our simulations, the standard deviation of the fracture length in all diversion cases was less than the value of the no diversion case, which demonstrates that perforation plugging can promote the uniformity of fracture length. The same phenomenon was also observed in the fluid distribution in the fractures (Fig. 23b). In the diversion cases, with the increase in the number of diverters, the standard deviation of fracture length decreased continuously, and the fracture length became uniform. But the uniform fluid volume in each fracture did not mean the uniform fracture length, especially for the internal fracture. To obtain a more uniform fracture length, the internal fracture usually requires more subsequent fracturing fluid, and then more aggressive measures should be applied (such as increasing the number of diverters or advancing the diverting timing). With the delay of diverting timing, the standard deviation of fracture length decreased at first and then increased. This change was mainly that, if the diverting timing is too early, the internal fracture before diversion will become the superior fracture after diversion; if the diverting timing is too late, the internal fracture before diversion could not get enough fracturing fluid due to the limited subsequent fracturing time. Neither of these two situations could promote the uniform propagation of multiple fractures. It is worth noting that when the total number of

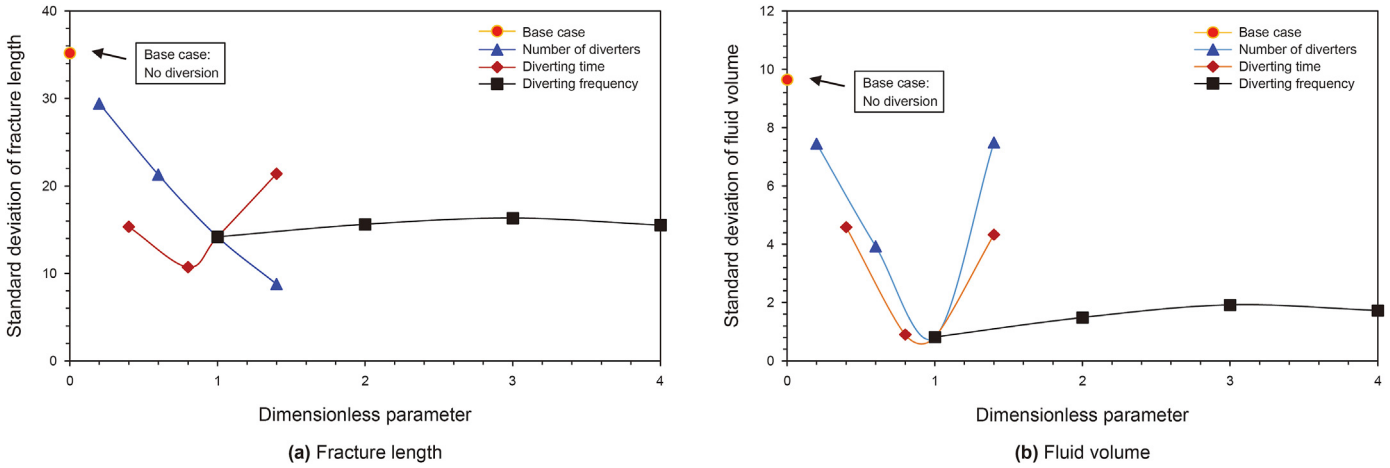

Fig. 23. The standard deviation of fracture length and fluid volume with different dimensionless diversion parameters.

diverters was the same, increasing the injection frequency of diverters in this study had little effect on the uniformity of fracture propagation. Besides, our research only studied the diversion cases when certain parameter changes. In the future, we will try to combine several plugging parameters to promote a more uniform fracture propagation. Meanwhile, our simulation also showed that, even if the optimized temporary plugging case promoted the uniformity of injection fluid volume in each fracture, the uniformity of the fracture length still shows great instability. Recently, Dontsov and Suarez-Rivera (2020) also showed that the morphology of multiple fractures with uniform fluid injection varies greatly under the different propagation mechanisms. For example, in the viscosity-dominant regime, the morphology of multi-cluster fractures was nearly identical and radially symmetric, while in the roughness-dominant regime, multi-clusters interacted strongly and the fracture geometry was similar to that of petals in a flower. These phenomena indicate that the multi-cluster fracture presents greater propagation instability. Based on the multiple hypotheses in this study, the multi-fracture propagation under the perforation plugging condition still needs more research. For example, our conclusions may not be applicable for other special models (e.g., stress inhomogeneous or fractured reservoirs). Meanwhile, A more realistic rock model should be considered to provide more meaningful guidelines for practical applications in further work.

6. Conclusions

A fluid-solid fully coupled three-dimensional finite element model with the CZM model was established to simulate the propagation of multiple fractures during ITPF. Based on the fluid pipe element and its subroutine, this model can fully consider the flow partitioning before and after perforation plugging. Meanwhile, this model has been verified by the analytical solution. The effects of the number of diverters, diverting timing, and injection frequency on the uniformity of multi-fracture propagation were also investigated. The main conclusions can be drawn based on our simulations:

(1) The behavior of perforation plugging could eliminate the effect of stress interference between multiple fractures and promote a uniform fracture propagation and fluid distribution, whose mechanism is that the perforation plugging changes the original distribution of the number of perforations, thus changing the flux partitioning after the diverting time.
(2) Compared to the base case, the diversion case has a more uniform fluid distribution of multiple fractures, and the standard deviation of fluid distribution in the diversion case was only 8.48% of that in the base case.
(3) Injecting more diverters will create a higher plugging pressure rise during ITPF, which will increase the risk of wellbore integrity. Comprehensively considering pressure rise and fluid distribution, the number of diverters should be 50% of the total number of perforations (N_{pt}), whose standard deviation of the fluid distribution of multiple fractures was lower than those in the cases of injecting 10%N_{pt}, 30%N_{pt} and 70%N_{pt}.
(4) Injecting diverters at different diverting timings will get the same plugging pressure rise, but the fluid distribution is very different. The diverters should be injected at an appropriate timing, i.e. 40% or 50% of the total fracturing time(t_{ft}), when the standard deviation of the fluid distribution of multiple fractures was only about 20% of standard deviations in the cases of injecting at 20%t_{ft} or 70%t_{ft}.
(5) A single injection with all diverters is better than multiple injections because a single injection can maintain high bottom-hole pressure for a longer period and promote a more uniform fluid distribution. The standard deviation of the fluid distribution in a single injection case was 43.62%–55.41% of the other cases with multiple injection cases.

Acknowledgments

This work is financially supported by the National Natural Science Foundation of China (No. 52174045, No. 52104011) and Natural Science Foundation of Xinjiang Uygur Autonomous Region (2022D01B77).

References

Brown, R., Neill, G., Zhang, X., 1963. Factors influencing optimum ball sealer performance. J. Petrol. Technol. 15 (4), 450–454. https://doi.org/10.2118/553-PA.
Chen, M., Zhang, S., Xu, Y., et al., 2020a. A numerical method for simulating planar 3D multi-fracture propagation in multi-stage fracturing of horizontal wells. Petrol. Explor. Dev. 47 (1), 171–183. https://doi.org/10.1016/S1876-3804(20)60016-7.
Chen, M., Zhang, S., Zhou, T., et al., 2020b. Optimization of in-stage diversion to promote uniform planar multifracture propagation: a numerical study. SPE J. 25 (6), 3091–3110. https://doi.org/10.2118/201114-PA.
Chen, Z., Bunger, A.P., Zhang, X., et al., 2009. Cohesive zone finite element-based

modeling of hydraulic fractures. Acta Mech. Solida Sin. 22, 443–452. https://doi.org/10.1016/S0894-9166(09)60295-0.
Chen, Z., 2012. Finite element modelling of viscosity-dominated hydraulic fractures. J. Petrol. Sci. Eng. 89, 136–144. https://doi.org/10.1016/j.petrol.2011.12.021.
Cipolla, C., Weng, X., Mack, M., et al., 2011. Integrating microseismic mapping and complex fracture modeling to characterize hydraulic fracture complexity. In: SPE Hydraulic Fracturing Technology Conference. https://doi.org/10.2118/140185-MS.
Cramer, D., 1987. The application of limited-entry techniques in massive hydraulic fracturing treatments. SPE Prod. Operat. Symp. https://doi.org/10.2118/16189-MS.
Cramer, D., Friehauf, K., Roberts, G., et al., 2020. Integrating distributed acoustic sensing, treatment-pressure analysis, and video-based perforation imaging to evaluate limited-entry-treatment effectiveness. SPE Prod. Oper. 26, 1855–1862. https://doi.org/10.2118/194334-PA.
Crump, J., Conway, M., 1988. Effects of perforation-entry friction on bottomhole treating analysis. J. Petrol. Technol. 40 (8), 1041–1048. https://doi.org/10.2118/15474-PA.
Dontsov, E.V., Suarez-Rivera, R., 2020. Propagation of multiple hydraulic fractures in different regimes. Int. J. Rock Mech. Min. 128, 104270. https://doi.org/10.1016/j.ijrmms.2020.104270.
EIA, 2018. Annual Energy Outlook 2018. U.S. Energy Information Administration.
Erbstoesser, S., 1980. Improved ball sealer diversion. J. Petrol. Technol. 32 (11), 1903–1910. https://doi.org/10.2118/8401-PA.
Fragachán, F., Shahri, M., Arnold, D., et al., 2016. In: Enhancing well performance via in-stage diversion in unconventional wells: physics and case studies. https://doi.org/10.2118/180985-MS. SPE Argentina Exploration and Production of Unconventional Resources Symposium.
Guo, J., Luo, B., Lu, C., et al., 2017. Numerical investigation of hydraulic fracture propagation in a layered reservoir using the cohesive zone method. Eng. Fract. Mech. 186, 195–207. https://doi.org/10.1016/j.engfracmech.2017.10.013.
Huang, J., Safari, R., Fragachan, F., 2018. Applications of self-degradable particulate diverters in wellbore stimulations: hydraulic fracturing and matrix acidizing case studies. In: SPE International Hydraulic Fracturing Technology Conference and Exhibition. https://doi.org/10.2118/191408-18IHFT-MS.
Kumar, D., Ghassemi, A., 2018. Three-dimensional poro-elastic modeling of multiple hydraulic fracture propagation from horizontal wells. Int. J. Rock Mech. Min. 105, 192–209. https://doi.org/10.1016/j.ijrmms.2018.01.010.
Lagrone, K., Rasmussen, J., 1963. A new development in completion methods- the limited entry technique. J. Petrol. Technol. 15 (7), 695–702. https://doi.org/10.2118/530-PA.
Lecampion, B., Desroches, J., 2015. Simultaneous initiation and growth of multiple radial hydraulic fractures from a horizontal wellbore. J. Mech. Phys. Solid. 82, 235–258. https://doi.org/10.1016/j.jmps.2015.05.010.
Li, X., Chen, Z., Chaudhary, S., et al., 2005. An integrated transport model for ball-sealer diversion in vertical and horizontal wells. In: SPE Annual Technical Conference and Exhibition. https://doi.org/10.2118/96339-MS.
Li, Y., Deng, J., Liu, W., et al., 2017. Numerical simulation of limited-entry multi-cluster fracturing in horizontal well. J. Petrol. Sci. Eng. 152, 443–455. https://doi.org/10.1016/j.petrol.2017.03.023.
Long, G., Liu, S., Xu, G., et al., 2018. A perforation-erosion model for hydraulic-fracturing applications. SPE Prod. Oper. 33 (4), 770–783. https://doi.org/10.2118/174959-PA.
Li, J., Dong, S., Wen, H., et al., 2020. Numerical simulation of temporarily plugging staged fracturing (TPSF) based on cohesive zone method. Comput. Geotech. 121, 103453. https://doi.org/10.1016/j.compgeo.2020.103453.
Li, M., Zhou, F., Yuan, L., et al., 2021. Numerical modeling of multiple fractures competition propagation in the heterogeneous layered formation. Energy Rep. 7, 3737–3749. https://doi.org/10.1016/j.egyr.2021.06.061.
Li, M., Lv, W., Liu, J., et al., 2022a. Effect of perforation friction on 3D In-stage multiple fracture propagation: a numerical study. Eng. Fract. Mech. 267, 108415. https://doi.org/10.1016/j.engfracmech.2022.108415.
Li, M., Zhou, F., Liu, J., et al., 2022b. Quantitative Investigation of Multi-Fracture Morphology during TPDF through True Tri-axial Fracturing Experiments and CT Scanning. Petrol Sci., 2022.
Li, M., Zhou, F., Sun, Z., et al., 2022c. Experimental study on plugging performance and diverted fracture geometry during different temporary plugging and diverting fracturing in Jimusar shale. J. Petrol. Sci. Eng. https://doi.org/10.1016/j.petrol.2022.110580, 110580.
Mayerhofer, M., Lolon, E., Warpinski, N., et al., 2008. What is stimulated rock volume?. In: SPE Shale Gas Production Conference https://doi.org/10.2118/119890-MS.
Miller, C., Waters, G., Rylander, E., 2011. Evaluation of production log data from horizontal wells drilled in organic shales. In: The North American Unconventional Gas Conference and Exhibition. https://doi.org/10.2118/144326-MS.
Nozaki, M., Zhu, D., Hill, A., 2013. Experimental and field data analysis of ball-sealer diversion. SPE Prod. Oper. 28, 286–295. https://doi.org/10.2118/147632-PA.
Panjaitan, M., Moriyama, A., McMillan, D., et al., 2018. Qualifying diversion in multi clusters horizontal well hydraulic fracturing in haynesville shale using water hammer analysis, step-down test and microseismic data. In: SPE Hydraulic Fracturing Technology Conference and Exhibition. https://doi.org/10.2118/189850-MS.
Rahim, Z., Al-Kanaan, A., Taha, S., et al., 2017. Innovative diversion technology ensures uniform stimulation treatments and enhances gas production: example from carbonate and sandstone reservoirs. In: SPE Hydraulic Fracturing Technology Conference and Exhibition. https://doi.org/10.2118/184840-MS.
Ramurthy, M., Richardson, J., Brown, M., et al., 2016. Fiber-optics results from an intra-stage diversion design completions study in the niobrara formation of DJ Basin. In: SPE Hydraulic Fracturing Technology Conference. Society of Petroleum Engineers. https://doi.org/10.2118/179106-MS.
Raterman, K., Farrell, H., Mora, O., et al., 2018. Sampling a stimulated rock volume: an Eagle Ford example. SPE Reservoir Eval. Eng. 21, 927–941. https://doi.org/10.2118/191375-PA.
Roberts, G., Whittaker, J., McDonald, J., 2018. A novel hydraulic fracture evaluation method using downhole video images to analysis perforation erosion. In: SPE International Hydraulic Fracturing Technology Conference and Exhibition. https://doi.org/10.2118/191466-18IHFT-MS.
Roberts, G., Whittaker, J., McDonald, J., et al., 2020. Proppant distribution observations from 20,000+ perforation erosion measurements. In: SPE Hydraulic Fracturing Technology Conference and Exhibition. https://doi.org/10.2118/199693-MS.
Senters, C., Johnson, M., Leonard, R., et al., 2018. Diversion optimization in new well completions. In: SPE Hydraulic Fracturing Technology Conference and Exhibition. https://doi.org/10.2118/189900-MS.
Shin, D., Sharma, M., 2014. Factors controlling the simultaneous propagation of multiple competing fractures in a horizontal well. In: Proceedings of the SPE Hydraulic Fracturing Technology Conference. Society of Petroleum Engineers. https://doi.org/10.2118/168599-MS.
Simulia, D., 2019. Abaqus 6.14 User's Manual, Dassault Systems, Providence, RI.
Somanchi, K., O'Brien, C., Huckabee, P., et al., 2016. Insights and observations into limited entry perforation dynamics from fiber-optic diagnostics. In: The Unconventional Resources Technology Conference. https://doi.org/10.15530/URTEC-2016-2458389.
Taleghani, A.D., Miguel, G., Yu, H., et al., 2018. Numerical simulation of hydraulic fracture propagation in naturally fractured formations using the cohesive zone model. J. Petrol. Sci. Eng. 165, 42–57. https://doi.org/10.1016/j.petrol.2018.01.063.
Ugueto, C., Huckabee, P., Molenaar, M., et al., 2016. Perforation cluster efficiency of cemented plug and perf limited entry completions: insights from fiber optics diagnostics. In: SPE Hydraulic Fracturing Technology Conference. https://doi.org/10.2118/179124-MS.
Vidma, K., Abivin, P., Dunaeva, A., et al., 2018. Far-field diversion technology to prevent fracture hits in tightly spaced horizontal wells. In: SPE Annual Technical Conference and Exhibition. https://doi.org/10.2118/191722-MS.
Wang, B., Zhou, F., Yang, C., et al., 2020a. Experimental study on injection pressure response and fracture geometry during temporary plugging and diverting fracturing. SPE J. 25, 573–586. https://doi.org/10.2118/199893-PA.
Wang, D., Dong, Y., Sun, D., et al., 2020b. A three-dimensional numerical study of hydraulic fracturing with degradable diverting materials via CZM-based FEM. Eng. Fract. Mech. 237, 107251. https://doi.org/10.1016/j.engfracmech.2020.107251.
Weddle, P., Griffin, L., Pearson, C., 2018. Mining the Bakken II - pushing the envelope with extreme limited entry perforating. In: SPE Hydraulic Fracturing Technology Conference and Exhibition. https://doi.org/10.2118/189880-MS.
Weijers, L., Wright, C., Mayerhofer, M., et al., 2019. Trends in the North American frac industry: invention through the shale revolution. In: SPE Hydraulic Fracturing Technology Conference and Exhibition. https://doi.org/10.2118/194345-MS.
Wheaton, B., Haustveit, K., Deeg, W., et al., 2016. A case study of completion effectiveness in the Eagle Ford shale using DAS/DTS observations and hydraulic fracture modeling. In: SPE Hydraulic Fracturing Technology Conference. https://doi.org/10.2118/179149-MS.
Wheaton, B., Miskimins, J., Wood, D., 2014. Integration of distributed temperature and distributed acoustic survey results with hydraulic fracture modeling: a case study in the woodford shale. In: The Unconventional Resources Technology Conference. https://doi.org/10.15530/urtec-2014-1922140.
Wu, K., Olson, J., 2015. Simultaneous multi-frac treatments: fully coupled fluid flow and fracture mechanics for horizontal wells. SPE J. 20, 337–346. https://doi.org/10.2118/167626-STU.
Wu, K., Olson, J., 2016. Mechanisms of simultaneous hydraulic-fracture propagation from multiple perforation clusters in horizontal wells. SPE J. 21, 1000–1008. https://doi.org/10.2118/178925-PA.
Wu, K., Olson, J., Balhoff, M., et al., 2017. Numerical analysis for promoting uniform development of simultaneous multiple fracture propagation in horizontal wells. SPE Prod. Oper. 32 (1), 41–50. https://doi.org/10.2118/174869-PA.
Yang, C., Zhou, F., Feng, W., et al., 2019. Plugging mechanism of fibers and particulates in hydraulic fracture. J. Petrol. Sci. Eng. 176, 396–402. https://doi.org/10.1016/j.petrol.2019.01.084.
Yu, H., Taleghani, A.D., Lian, Z., et al., 2019. On how pumping hesitations may improve complexity of hydraulic fractures, a simulation study. Fuel 249, 294–308. https://doi.org/10.1016/j.fuel.2019.02.105.
Yuan, L., Zhou, F., Li, B., et al., 2020. Experimental study on the effect of fracture surface morphology on plugging efficiency during temporary plugging and diverting fracturing. J. Nat. Gas Sci. Eng. 81, 103459. https://doi.org/10.1016/j.jngse.2020.103459.
Zeng, Q., Liu, Z., Wang, T., Gao, Y., et al., 2017. Fully coupled simulation of multiple hydraulic fractures to propagate simultaneously from a perforated horizontal wellbore. Comput. Mech. 61, 137–155. https://doi.org/10.1007/s00466-017-1412-5.
Zhang, G., Liu, H., Zhang, J., et al., 2010. Three-dimensional finite element simulation

and parametric study for horizontal well hydraulic fracture. J. Petrol. Sci. Eng. 72, 310–317. https://doi.org/10.1016/j.petrol.2010.03.032.
Zhang, L., Zhou, F., Mou, J., et al., 2019. Large-scale true tri-axial fracturing experimental investigation on diversion behavior of fiber using 3D printing model of rock formation. J. Petrol. Sci. Eng. 181, 156–171. https://doi.org/10.1016/j.petrol.2019.06.035.
Zhao, J., Chen, X., Li, Y., et al., 2016. Simulation of simultaneous propagation of multiple hydraulic fractures in horizontal wells. J. Petrol. Sci. Eng. 147, 788–800. https://doi.org/10.1016/j.petrol.2016.09.021.
Zhou, F., Su, H., Liang, X., et al., 2019. Integrated hydraulic fracturing techniques to enhance oil recovery from tight rocks. Petrol. Explor. Dev. 46, 1065–1072. https://doi.org/10.1016/S1876-3804(19)60263-6.
Zou, Y., Ma, X., Zhang, S., 2020. Numerical modeling of fracture propagation during temporary-plugging fracturing. SPE J. 25, 1503–1522. https://doi.org/10.2118/199351-PA.